Wing Design by Numerical Optimization

Raymond M. Hicks*
NASA Ames Research Center, Moffett Field, Calif.
and
Preston A. Henne†
Douglas Aircraft Co., Long Beach, Calif.

A study was conducted to assess the feasibility of performing computerized wing design by numerical optimization. The design program combined a full-potential, inviscid aerodynamics code with a conjugate gradient optimization algorithm. Three design problems were selected to demonstrate the design technique. The first involved modifying the upper surface of the inboard 50% of a swept wing to reduce the shock drag subject to a constraint on wing volume. The second involved modifying the entire upper surface of the same swept wing (except the tip section) to increase the lift-drag ratio, subject to constraints on wing volume and lift coefficient. The final problem involved modifying the inboard 50% of a low-speed wing to achieve good stall progression. Results from the three cases indicate that the technique is sufficiently accurate to permit substantial improvement in the design objectives.

Nomenclature

a,b = participation coefficients
b = span
AR = aspect ratio
c_{d_s} = section shock plus thickness drag coefficient
c_l = section lift coefficient
C_R = root chord, m
C_T = tip chord, m
C_{D_I} = wing induced drag coefficient
C_{D_S} = wing shock drag coefficient
C_{D_T} = $C_{D_I} + C_{D_S}$
C_{D_P} = wing drag coefficient calculated by integration of surface pressures
C_L = wing lift coefficient
C_m = wing pitching moment coefficient
c_p = pressure coefficient, $(p_l - p)/q$
c_p^* = pressure coefficient for $M_l = 1$
f = airfoil shape function
h = shape function amplitude
M = Mach number
p = static pressure
q = dynamic pressure
x = nondimensional airfoil abscissa
y = nondimensional airfoil ordinate
α = angle of attack
η = nondimensional spanwise coordinate

Subscripts

l.s. = lower surface
u.s. = upper surface
L.E. = leading edge
l = local conditions
∞ = freestream conditions

Presented as Paper 77-1247 at the AIAA Aircraft Systems and Technology Conference, Seattle, Wash., Aug. 22-24, 1977; submitted Sept. 28, 1977; revision received April 7, 1977. Copyright © American Institute of Aeronautics and Astronautics, Inc., 1977. All rights reserved.

Index categories: Aerodynamics; Computational Methods; Analytical and Numerical Methods.

*Research Scientist. Member AIAA.
†Scientist Specialist. Member AIAA.

Introduction

OVER the last three years, a major effort has been underway to develop numerical optimization techniques for the design of airfoil sections for both low-speed and transonic applications.[1-8] The studies described in Refs. 1-8 clearly define those areas where design by numerical optimization is superior to design by inverse techniques. A principal advantage in using numerical optimization for two-dimensional design is that the designer is able to consider off-design conditions automatically during the design process. Such a capability has been demonstrated in the design of a supercritical airfoil section without "drag-creep."[8] Another advantage in the use of numerical optimization is that the method is readily extended to three dimensions. While this fact is conceptually clear, a study was needed to determine if three-dimensional aerodynamic codes generate consistent (free from random numerical error) aerodynamic coefficients. Consistency is required for the accurate calculation of gradient values by optimization algorithms. Such gradients define a direction of change in a given set of design variables to achieve a desired design improvement.

During the present study, the numerical optimization program described in Ref. 9 has been coupled to the aerodynamics program outlined in Ref. 10. The optimization code is based on the method of feasible directions and the aerodynamics code solves the three-dimensional potential equation for subsonic through transonic flow with exact boundary conditions. The aerodynamics code has been used successfully over a Mach number range from 0.1 to 0.95. The combination optimization-aerodynamic program has been applied to three-wing design problems to evaluate the adequacy of the technique to the design of practical wings for low-speed and transonic airplanes.

Design Method

Only a brief description of the numerical optimization process will be given here, since a complete discussion of the technique can be found in Ref. 9.

A schematic flow chart of the optimization process is depicted in Fig. 1. The hypothetical design problem shown in the figure is drag minimization with three design variables (h_1, h_2, h_3). The design variables can be thought of as jacks placed under the skin of the root profile with the ability to displace the skin up and down. The actual functions used to shape the wings considered during this study will be discussed

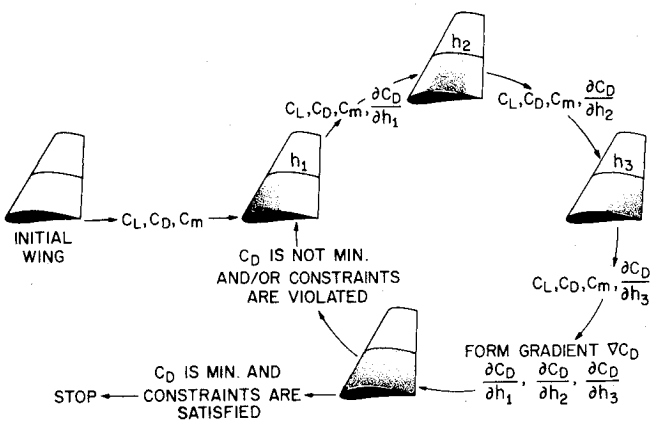

Fig. 1 Optimization flow chart for drag minimization with three design variables.

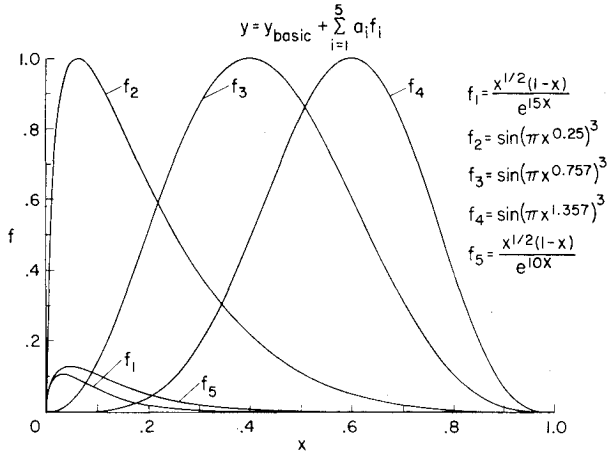

Fig. 2 Airfoil shape functions.

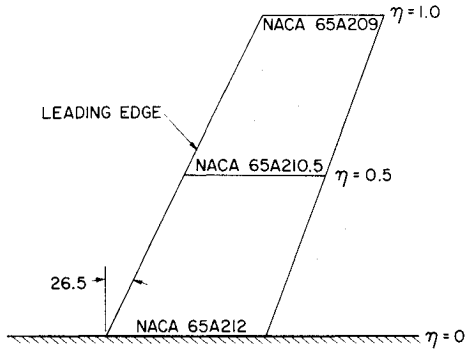

Fig. 3 Swept wing on a wall, $C_T/C_R = 0.75$, $\mathcal{R} = 4.57$.

in the next section. The shaded regions of the wing (Fig. 1) represent displacement of the skin upward between the root and the midspan station. The midspan and tip stations were considered fixed for this hypothetical design problem.

The first step in the design process is calculation of the aerodynamic coefficients of the initial wing. These coefficients are stored as baseline values for future use in the gradient calculations. The optimization program then perturbs each of the three jacks (design variables) one by one, returning to the aerodynamics program for evaluation of the aerodynamic coefficients and the partial derivative of drag with respect to each design variable after each perturbation. The partial derivatives form the gradient of drag (∇C_D). The direction in which the jacks are displaced to reduce the drag coefficient is $-\nabla C_D$ (the steepest descent direction). The optimization program increments the jacks one to four times in the direction indicated by $-\nabla C_D$. The process continues until the drag begins to increase due to nonlinearity in the design space or until a constraint, such as wing thickness, is encountered.

In the example depicted in Fig. 1, all jacks were displaced upward as required by the values of $-\nabla C_D$. If the drag begins to increase or a constraint is encountered, a new gradient is calculated and a new direction is found that will decrease drag without violating constraints. When a minimum value of drag is attained with constraints satisfied, the final wing geometry is printed along with the final pressure distributions and aerodynamic coefficients.

During this study, both momentum control volume integrations and surface pressure integrations were used to calculate aerodynamic coefficients. The control volume integrations utilized both far-field and near-field flow conditions to evaluate shock drag (C_{D_S}), induced drag (C_{D_I}), and lift coefficient (C_L). Surface pressure integrations were used to calculate a total drag coefficient (C_{D_P}) and pitching moment coefficient ($C_{M_{L.E.}}$). Spanwise distributions of section drag (c_{d_s}) include a spanwise distribution of drag due to airfoil thickness and finite span and section shock drag; c_{d_s} does not include the induced drag effects of the trailing vortex wake.

Design Variables

The airfoil shape at each span station can be represented by the following equations

$$y_{u.s.} = y_{u.s._{basic}} + \sum_{i=1}^{5} a_i f_i$$

$$y_{l.s.} = y_{l.s._{basic}} + \sum_{i=1}^{5} b_i f_i$$

where $y_{u.s._{basic}}$ and $Y_{l.s._{basic}}$ are the ordinates of the upper and lower surfaces of the baseline sections and f_i is the shape function shown in Fig. 2. The shape functions are added linearly to the baseline profiles by the optimization program to achieve the desired design improvement. The contribution of each function is determined by the value of the participation coefficients (design variables), a_i's and b_i's, associated with that function. All participation coefficients are initially set to zero, so the first computation gives the aerodynamic characteristics of the baseline wing. Therefore, the importance of each shape function in achieving the design improvement can be ascertained at any step during the optimization process by observing the value of the participation coefficient associated with each function at that step.

The shape functions shown in Fig. 2 were selected because of previous success in designing two-dimensional sections with functions of this type.[8] Three of the functions (f_1, f_2, f_5) have a predominant effect near the leading edge of the section. Such effect is desirable when supercritical sections are under consideration or when leading-edge pressure gradients must be controlled for stall progression.

Since this study was conducted to determine the feasibility of performing wing design by numerical optimization and was not intended to generate advanced wings, no attempt was made to find the best set of shape functions for three-dimensional design. Future effort will be devoted to the development of improved wing parameterization to give the designer more flexibility in wing optimization.

The primary design variables used during the study were the five functions shown in Fig. 2. In effect, these shape functions allow changes in both thickness and camber at the span stations where used. Other design variables as computationally efficient as those related to section geometry are twist and angle of attack, α; both twist and α were utilized during this study and were found to be useful design

variables. Planform variables, such as aspect ratio, taper, and sweep, could also be used as design variables. However, these parameters require a greater expenditure of computer time than the variables just mentioned when the flowfield equations are solved by finite-difference calculations, as in this study.

Design Results and Discussion

The primary objective of this investigation was to demonstrate the usefulness and versatility of numerical optimization in wing design. In addition to demonstrating the technique, three fundamental questions related to the suitability of the computed aerodynamic data for use with a gradient algorithm were considered. The three questions, listed in decreasing order of importance, are:

1) Are the aerodynamic coefficients calculated with sufficient consistency to reflect the effect of minute geometric change? (The answer to this question must be affirmative to obtain accurate gradient values for the optimization algorithm.)

2) How small must the velocity potential residuals generated by the finite-difference computation be to achieve the desired consistency mentioned in the first question? (Computer time is an inverse function of residual size.)

3) How fine must the finite-difference mesh be to give good flowfield definition, including shock capturing? (Computer time is a function of mesh spacing.)

Three different design problems were considered during this study in an effort to answer the preceding questions and to demonstrate the flexibility of the design technique. The primary results shown are for finite-difference aerodynamic calculations carried out on a mesh consisting of 60 streamwise, 10 vertical, and 12 spanwise mesh points. Iterations were terminated when the maximum residual multiplied by $(\Delta x)^2$ reached 10^{-5}. Since demonstration of the technique can be accomplished with results from coarse mesh calculations, only one of the three design problems was repeated with fine mesh calculations and for different convergence criteria to conserve computer time.

The first problem involved recontouring the inboard half of the upper surface of the swept wing shown in Fig. 3. The wing has an aspect ratio of 4.57 and has three defining airfoil sections at the nondimensional span stations (η) of 0, 0.5, and 1.0. NACA 6-series airfoil sections were used at each defining station with the thickness ratios indicated in the figure. The design objective was shock-drag reduction at Mach 0.85 and 1 deg angle of attack, subject to a lower bound constraint on wing volume. The five shape functions shown in Fig. 2 were used to modify the upper surface of the NACA 65A212 root section of the wing. The root section upper surface was described in the program by the following equation

$$y = y_{\text{basic}} + \sum_{i=1}^{5} a_i f_i$$

where the a_i's are the participation coefficient treated as design variables by the optimization program. Modification of the root profile affects all sections between the root and midspan through linear lofting in the program. The results of the modification are shown in Table 1. The shock-drag coefficient was reduced from 0.0039 to 0.0005, and the nose-down pitching moment was reduced nearly 30%. Little change occurred in the other aerodynamic coefficients.

Table 1 Inviscid aerodynamic coefficients for wing modification to reduce shock drag, $M = 0.85$, $\alpha = 1$ deg

	C_L	C_{D_I}	C_{D_S}	C_{D_T}	C_{D_P}	$C_{m_{\text{L.E.}}}$
Basic wing	0.22	0.0033	0.0039	0.0072	0.0070	−0.091
Modified wing	0.21	0.0030	0.0005	0.0035	0.0039	−0.065

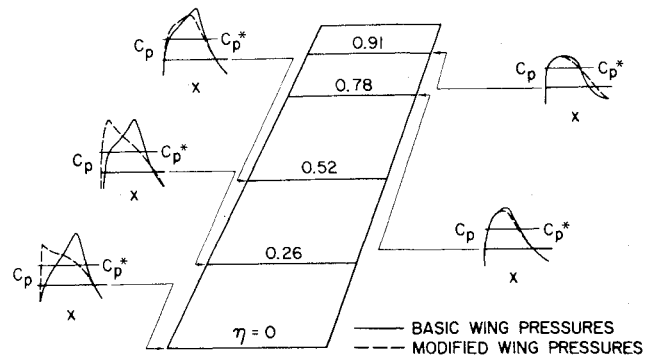

Fig. 4 Upper surface pressure distributions for wing modification to reduce shock drag, $M = 0.85$, $\alpha = 1$ deg.

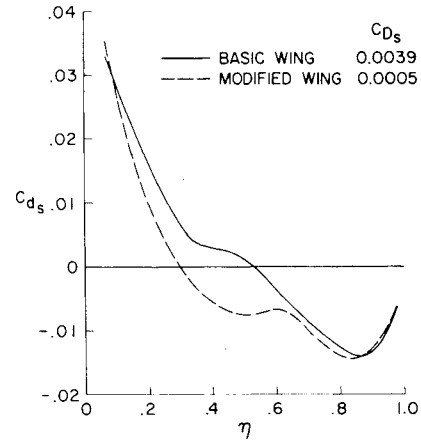

Fig. 5 Sectional shock-drag coefficients for wing modification to reduce shock drag, $M = 0.85$, $\alpha = 1$ deg.

Upper surface, chordwise, pressure distributions at five span stations for both the baseline and modified wings are shown in Fig. 4. Lower surface pressures were omitted for clarity and because little change in lower surface pressures resulted from the upper surface modification. As expected, the greatest pressure change occurred between the root and midspan stations, since the modification terminated at $\eta = 0.5$. However, small pressure changes did occur at least as far as $\eta = 0.91$ because of induced effects. Note that the strong aft shock of the root section of the baseline wing has been nearly eliminated by the modification. The modified pressure distribution is quite "peaky" and has a nearly isentropic compression.

It is interesting to compare the results of Fig. 4 with those of Fig. 5, a graph of section drag coefficient vs span station. The peculiar spanwise variation of c_{d_S} reflects the presence of a spanwise distribution of drag, due to airfoil thickness and finite span in addition to shock drag. The substantial reduction in shock strength on the inboard section of the wing (Fig. 4) is the result of softening or eliminating the shock wave due to the original airfoil geometry. Near $\eta = 0$, c_{d_S} is essentially unchanged. This result indicates the changes in shock drag and "thickness and span" drag are compensating. Because of limited time and computer funds, this design problem was not repeated on a refined mesh. Hence, it is impossible at this time to ascertain if this result is mesh-dependent.

A plot of sectional lift coefficients vs span station is shown in Fig. 6. As expected, most of the reduction in sectional lift

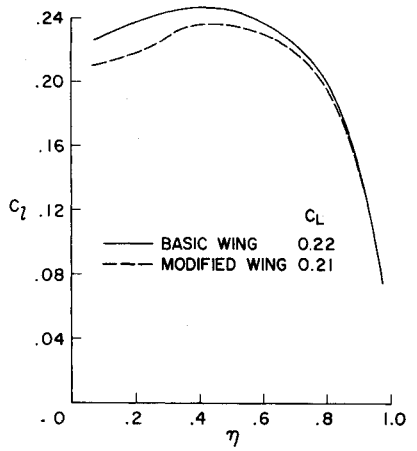

Fig. 6 Sectional lift coefficients for wing modification to reduce shock drag, $M = 0.85$, $\alpha = 1$ deg.

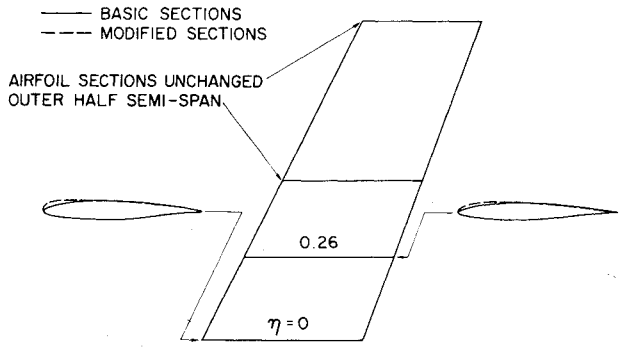

Fig. 7 Original and modified airfoil sections for wing modification to reduce shock drag.

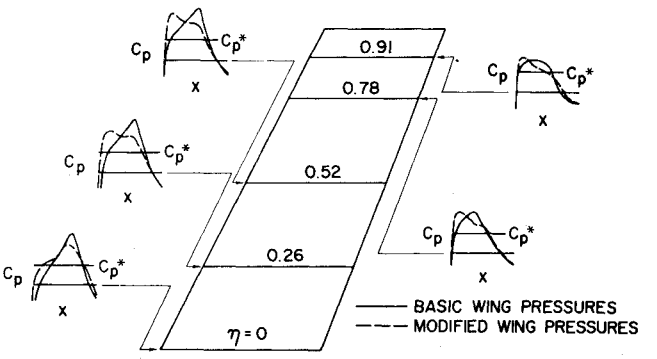

Fig. 8 Upper surface pressure distributions for wing modification to increase lift-drag ratio, $M = 0.85$.

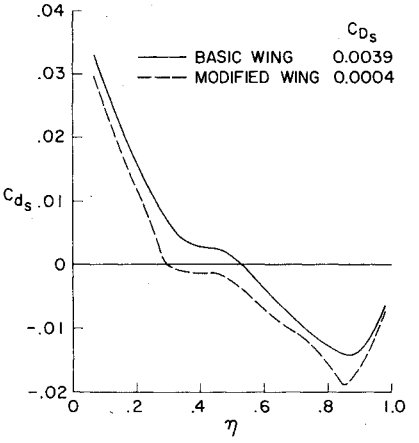

Fig. 9 Sectional shock-drag coefficients for wing modification to increase lift-drag ratio, $M = 0.85$.

coefficients occurred over the modified inboard wing sections.

Baseline and modified airfoil sections at two span stations are shown in Fig. 7. It appears that the root profile has excessive leading-edge bluntness which is consistent with the peaky pressure distribution shown in Fig. 4. The linear lofting between the root and the NACA 65A210.5 profile at midspan produced a more reasonable section at $\eta = 0.26$. If this had been an actual design problem, additional constraints could have been imposed on upper surface ordinates near the root leading edge to control the bluntness. The reduction in shock drag achieved for this example took two optimization iterations and 4 min on a CDC 7600 computer. This result indicates that the shock-drag coefficients calculated by the finite-difference aerodynamics code are consistent enough to permit determination of a gradient direction ($-\nabla C_{D_S}$) sufficiently accurate for optimization.

The second problem considered during this study involved modification of the upper surface of the swept wing used for the first problem, to increase the lift-drag ratio at $M = 0.85$, $\alpha = 1$ deg. Lower bound constraints were imposed on wing volume and lift coefficient ($C_L \geq 0.22$). The shape functions

Table 2 Inviscid aerodynamic coefficients for wing modification to increase lift-drag ratio, $M = 0.85$

	C_L	$C_{m_{L.E}}$	C_{D_I}	C_{D_S}	C_{D_T}	C_{D_P}	C_L/C_{D_T}	α, deg
Basic wing	0.22	−0.091	0.0033	0.0039	0.0072	0.0070	30.6	1.00
Modified wing	0.25	−0.079	0.0042	0.0004	0.0046	0.0044	54.4	1.25

Table 3 Mesh density effect on the inviscid aerodynamic coefficients for wing modification to increase lift-drag ratio, $M = 0.85$

	C_L	$C_{m_{L.E.}}$	C_{D_I}	C_{D_S}	C_{D_T}	C_{D_P}	C_L/C_{D_T}	α, deg
Coarse Mesh (60 × 10 × 12):								
Basic wing	0.22	−0.091	0.0033	0.0039	0.0072	0.0070	30.6	1.00
Modified wing	0.25	−0.079	0.0042	0.0004	0.0046	0.0044	54.4	1.25
Fine Mesh (120 × 20 × 24):								
Basic wing	0.24	−0.107	0.0037	0.0064	0.0101	0.0096	23.8	1.00
Modified wing	0.24	−0.095	0.0038	0.0022	0.0060	0.0053	40.0	0.93

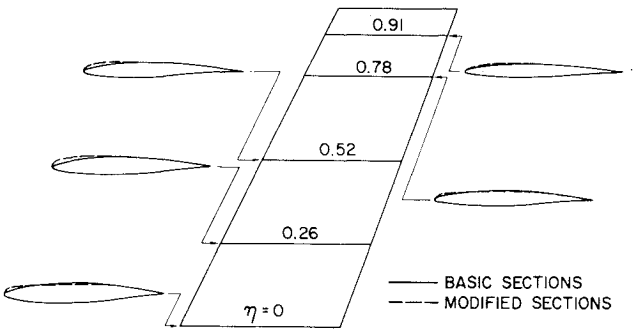

Fig. 10 Original and modified airfoil sections for wing modification to increase lift-drag ratio.

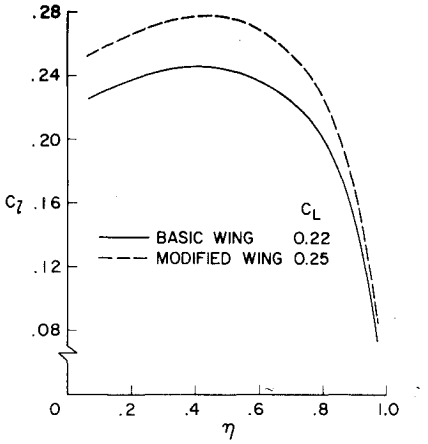

Fig. 11 Sectional lift coefficients for wing modification to increase lift-drag ratio, $M = 0.85$.

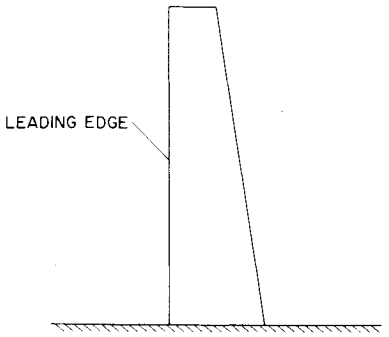

Fig. 12 Low-speed wing on a wall: $s = 180$ ft^2, $AR = 8.9$, $b = 40$ ft, $C_T/C_R = 0.5$ GAW – 2 airfoil section, no twist.

of Fig. 2 were used to perturb the upper surface ordinates at both the root and midspan sections to achieve the desired improvement in lift-drag ratio. Hence, linear lofting produced modification to all wing sections except the tip. The upper surface at the root and midspan stations were described in the program by the following equations:

Root:

$$y = y_{\text{basic}} + \sum_{i=1}^{5} a_i f_i$$

Midspan:

$$y = y_{\text{basic}} + \sum_{i=1}^{5} b_i f_i$$

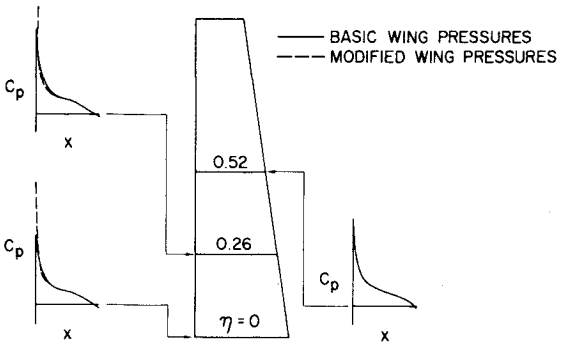

Fig. 13 Upper surface pressure distributions for wing modification to improve stall progression, $M = 0.1$, $\alpha = 12$ deg.

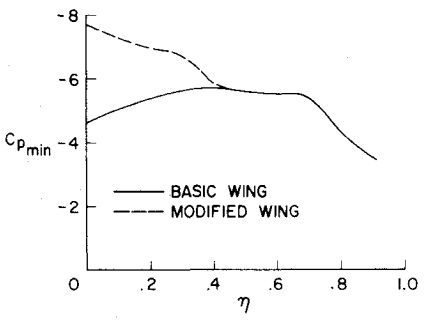

Fig. 14 Spanwise variation of minimum upper surface pressure coefficient for wing modification to improve stall progression, $M = 0.1$, $\alpha = 12$ deg.

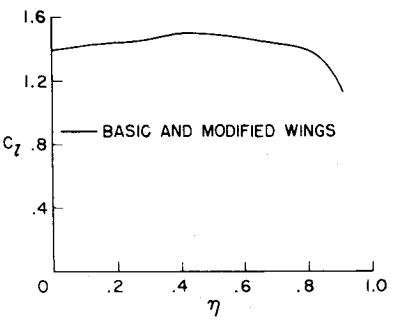

Fig. 15 Spanwise variation of sectional lift coefficients for wing modification to improve stall progression, $M = 0.1$, $\alpha = 12$ deg.

where the a_i's and b_i's are the participation coefficients (design variables) used by the optimization program. Angle of attack was also treated as a design variable for this problem, giving a total of eleven design variables.

The results of this modification are shown in Table 2. The increase in lift-drag ratio (the design objective) was due primarily to a reduction in C_{D_S}. Lift coefficient increased from 0.22 to 0.25, which accounts for the increase in C_{D_I}. This increase was accomplished primarily by increasing the angle of attack from 1 to 1.25 deg.

Upper surface pressure distributions at five span stations for both the baseline and modified wings are shown in Fig. 8. It is interesting to note that the smallest pressure change occurred at the root station, unlike the preceding example (Fig. 4). The other four pressure distributions show considerable change as expected, since nearly the entire upper surface was modified.

A graph of shock-drag coefficient vs span station is shown in Fig. 9. Unlike the results shown in Fig. 5, all wing sections, with the possible exception of the tip, show a reduction in C_{D_S} because of the modifications. The compensating drag effects

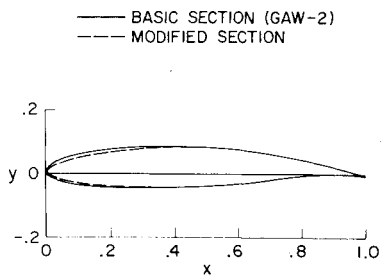

Fig. 16 Root airfoil sections for wing modification to improve stall progression.

at the root section noted in the previous example (Fig. 5) did not occur here because of a smaller amount of leading-edge bluntness generated at the root for the current example (Fig. 10). In spite of a relatively small section change at $\eta = 0.91$, the pressure distribution shows a fairly substantial change at this station (Fig. 8). As noted before, induced effects are quite important.

Pressure distributions at three span stations for both basic and modified wings are shown in Fig. 13. The minimum pressure peak at the leading edge of the root section decreased substantially, which should cause a decrease in stalling angle for this section and promote root stall. As expected, the lofting between the modified root section and the GAW-2 midspan section produced a smaller change in minimum pressure peak with increasing η.

A graph of minimum pressure peak vs span station is shown in Fig. 14 for both basic and modified wings. If magnitude of the leading-edge pressure peak is a good measure of stall progression, this figure shows that the initial stall has been moved from midspan to the root by the modification developed here.

The spanwise variation of sectional lift coefficient for the basic and modified wings is shown in Fig. 15. In spite of the large change in pressure peaks shown in the preceding figure, the sectional lift coefficients remained unchanged within the precision of the graph shown. This result implies that this type of modification can be accomplished without affecting the span loading or the induced drag of the baseline wing.

The root airfoil sections for the baseline and modified wings are shown in Fig. 16. The increased magnitude of the pressure peaks shown in Fig. 13 was generated by reducing the leading-edge radius and forward chamber of the GAW-2 airfoil section. Note that most of the change occurred on the upper surface.

Concluding Remarks

A practical, automated design technique with three-dimensiofal capability has been demonstrated, and several areas in need of further work has been identified. In particular, more work is needed to:

1) Define the smallest acceptable mesh density that will give reliable aerodynamic data for numerical optimization.

2) Define the least stringent velocity potential convergence criteria consistent with good aerodynamic data.

3) Develop accelerated convergence difference schemes for solving the three-dimensional potential equation for transonic flow.

4) Develop improved parameterization of the wing geometry to give more flexibility in achieving optimum wing geometry.

With the present design code, an optimization problem will require approximately 1 hour on a CDC 7600 computer for one flight condition and eleven design variables.

From the AIAA Progress in Astronautics and Aeronautics Series . . .

RADIATION ENERGY CONVERSION IN SPACE—v. 61

Edited by Kenneth W. Billman, NASA Ames Research Center, Moffett Field, California

The principal theme of this volume is the analysis of potential methods for the effective utilization of solar energy for the generation and transmission of large amounts of power from satellite power stations down to Earth for terrestrial purposes. During the past decade, NASA has been sponsoring a wide variety of studies aimed at this goal, some directed at the physics of solar energy conversion, some directed at the engineering problems involved, and some directed at the economic values and side effects relative to other possible solutions to the much-discussed problems of energy supply on Earth. This volume constitutes a progress report on these and other studies of SPS (space power satellite systems), but more than that the volume contains a number of important papers that go beyond the concept of using the obvious stream of visible solar energy available in space. There are other radiations, particle streams, for example, whose energies can be trapped and converted by special laser systems. The book contains scientific analyses of the feasibility of using such energy sources for useful power generation. In addition, there are papers addressed to the problems of developing smaller amounts of power from such radiation sources, by novel means, for use on spacecraft themselves.

Physicists interested in the basic processes of the interaction of space radiations and matter in various forms, engineers concerned with solutions to the terrestrial energy supply dilemma, spacecraft specialists involved in satellite power systems, and economists and environmentalists concerned with energy will find in this volume many stimulating concepts deserving of careful study.

690 pp., 6 × 9, illus., $24.00 Mem. $45.00 List

TO ORDER WRITE: Publications Dept., AIAA, 1290 Avenue of the Americas, New York, N. Y. 10019